Proceedings of Meetings on Acoustics

Volume 27 http://acousticalsociety.org/

Fourth International Conference on the Effects of Noise on Aquatic Life

Dublin, Ireland
10-16 July 2016

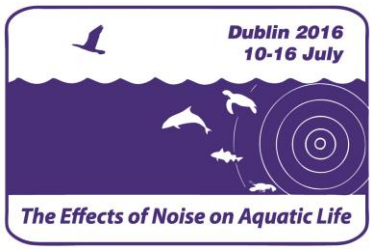

Soundscape characterization in a dynamic acoustic environment: Grand Passage, Nova Scotia, a planned in-stream tidal energy site

Anne R. Lombardi, Alex E. Hay and David R. Barclay
Department of Oceanography, Dalhousie University, Halifax, Nova Scotia, Canada;
anne.lombardi@dal.ca, alex.hay@dal.ca, dbarclay@dal.ca

The marine environment in the Bay of Fundy hosts a dynamic and diverse soundscape that is a fundamental component of the local ecosystem. The emergence of new human marine activities and infrastructure, such as tidal turbine installations, introduces new sound sources that change or disrupt the existing acoustic environment, but the full extent of these changes is not well understood and is not predictable. To better evaluate the effects of future tidal energy development on the local soundscape in Grand Passage, Nova Scotia, a thorough understanding of the pre-development characteristics must be established. The present research seeks to identify existing anthropophony, biophony, and geophony, and to evaluate the underlying mechanisms contributing to geophonic variability. Passive acoustic measurements have been conducted using long-term moored omnidirectional hydrophones, a moored 5-channel array, and drifting hydrophone arrays, enabling identification of dominant signals and source direction, estimation of pseudonoise masking effects due to turbulent flow, and analysis of diurnal, daily, seasonal, and annual variability as well as spatial variability within the study area. This paper provides an overview of the dominant sound sources and discusses the effects of environmental forcing on soundscape characteristics.

Published by the Acoustical Society of America

 [DOI: 10.1121/2.0000246]

1. INTRODUCTION

The conversion of kinetic energy from tidal flows into electrical energy has recently become a reality, with the installation of tidal energy turbines in the UK, France and several planned installations in the Bay of Fundy. The introduction of in-stream tidal energy conversion (TEC) devices into the marine environment can have an impact on local environmental characteristics, such as flow dynamics, seabed properties, benthic organisms, and marine mammals. As the industry progresses, continued research is necessary to ensure that any such impacts are known and actively minimized, and that environmental changes are effectively monitored over time.

Underwater noise associated with tidal energy, including noise from turbines and mooring infrastructure as well as noise from construction/maintenance, has potential implications for marine mammals that use sound for communication or navigation, and for other organisms that may be negatively impacted by increased acoustic energy and/or pressure levels. In addition, the source level and transmission of TEC-generated noise has implications for both the detection of hazards by marine life and for local marine mammal monitoring using passive acoustics. To quantify the noise introduced by tidal energy development activities, and to assess its detectability within the local environment, knowledge of pre-development baseline conditions must be established. However, as evidenced by the increased research focus on soundscapes and the role of sound in marine ecosystems (e.g. Williams *et al.*, 2014; Erbe *et al.*, 2015), traditional "baseline" ambient noise concepts and measurement approaches do not adequately address the variability in underlying sound production and propagation mechanisms that ultimately govern the local acoustic environment. Alternatively, the "baseline" becomes a compilation of various acoustic features that systematically represent a complex, dynamic soundscape.

Soundscape characterization in areas suitable for tidal energy is inherently challenging due to (1) pseudonoise contamination from turbulent flows; (2) increased broadband noise from mobile sediments in bedload motion or saltation; (3) variability of sound sources in coastal and near-coastal regions; and (4) complexity of propagation regimes in shallow water environments. The approach, including both instrumentation and analysis, must therefore address these challenges through mitigation of contamination effects and evaluation of noise over a broad range of frequencies, timescales, and spatial dimensions.

With high flow speeds and shallow bathymetry, the marine environment in Grand Passage (and nearby tidal channels Petit Passage and Digby Gut) has high potential for small-scale tidal energy development (Hay *et al.*, 2013a); all three passages have been granted a tidal power development license by the Nova Scotia government. The strong flows in the Bay of Fundy provide not only a renewable energy resource, but also a dynamic, nutrient-rich ecosystem supporting a variety of marine organisms, several active fisheries, and significant levels of recreational traffic from whale watching expeditions. Geographically, the outer Bay of Fundy provides marine access to several ports and fishing communities, including the port of Saint John, New Brunswick. The soundscape throughout the Bay is thus complex and dynamic, with a significant anthropophonic contribution from vessel traffic and a diverse biophonic contribution from marine mammals; within the Grand Passage environment, this complexity is amplified by the channel geometry, concentrated human activity, and elevated current speeds. A first approach to comprehensive characterization has therefore been conducted to provide a better understanding of the dynamic soundscape; to support effective monitoring of biological and anthropogenic sources; and to enable an assessment of the potential acoustic impacts of future tidal energy development in the area.

The research is focused on two main objectives: first, the identification of geo-, bio-, and anthropophonic soundscape contributors, and second, the evaluation of spatial and temporal variability in soundscape geophony based on underlying acoustic mechanisms. Passive acoustic datasets were collected using both drifting and moored hydrophones, and were analyzed concurrently with supplementary records of flow speed, acoustic backscatter, seabed video, and meteorological observations (section 2). The results, outlined in section 4, present an initial assessment of the relation between the natural physical environment and the acoustic environment, addressing the relevant sound sources as well as sound generation processes.

2. BACKGROUND AND METHODS

A. SITE DESCRIPTION

Separating Long Island to the East and Brier Island to the West, Grand Passage (figure 1) is characterized by strong currents driven by the large tidal range in the Bay of Fundy. The channel is approximately 4 km long and 1 km wide at its widest point, with depths between 10-30 m and a variable seabed composed of exposed bedrock, gravel/sand, cobbles, and shell fragments. A small island (Peter's Island) is located near the Southern entrance.

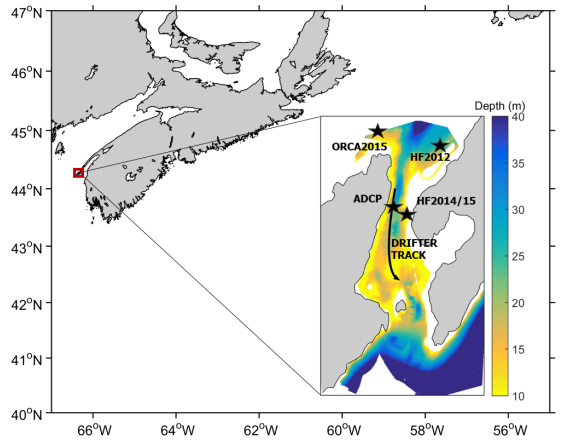

FIG. 1: Grand Passage is located in Southwest Nova Scotia, near the Grand Manan channel in the Bay of Fundy. The inset shows passage bathymetry and instrument locations.

Depth-averaged currents in many parts of the channel reach speeds up to 2 m/s, with peak locations exceeding 2.5 m/s (Hay *et al.*, 2013a,b). There is an observed asymmetry in flood (northward) and ebb (southward) current velocity, as well as spatial variability over the channel length; ebb currents are generally stronger, and the highest speeds have been recorded in the Southern half of the passage, in the narrow channel between Peter's Island and Long Island.

Surface roughness in Grand Passage is, on average, minimal, with low incidence of wind-driven breaking waves; small whitecaps are often observed, but propagating breaking waves do not form under average weather conditions. During storm events, by contrast, significant wave action can develop, with heights up to 2-3 m and 6-7 second periods for winter storms (A. Hay, personal communication). Due to the limited fetch, breaking waves typically form only when the wind and current directions are in opposition; seasonality in wind patterns therefore results in a temporal variation of the tidal dependence of wind-driven breaking waves in the Passage.

i. Marine mammal population

The coast of Southwest Nova Scotia is a region of diverse marine life, where the nutrient-rich waters of the Bay of Fundy support various species of both fish and mammals. Local marine mammal population data has been compiled based on several years' records (2005-2013) from whale watching cruises as well as a "citizen-science" observation program in 2014-15. The compiled data show an active marine mammal environment at the Northern entrance to Grand Passage, extending Westward past Brier Island (Malinka *et al.*, 2015a). Within the passage, sightings of larger mammals are infrequent but do occur; the population is typically dominated by harbor porpoise and pinnipeds. Table I summarizes results pertaining to

Class	Species	Occurrence	Species at Risk Status
Odontocetes	Atlantic white-sided dolphin	Common	None
	White-beaked dolphin	Rare	None
	Harbour Porpoise	Common	Threatened
	Long-finned Pilot whale	Common	None
	Killer whale	Rare	None
	Sperm whale	Rare	None
Mysticetes	North Atlantic right whale	Common	Endangered
	Humpback whale	Common	Special Concern
	Fin whale	Common	Special Concern
	Minke whale	Common	None
	Blue whale	Rare	Endangered
	Sei whale	Common	Endangered
Pinnipeds	Grey Seal	Common	None
	Harbour Seal	Common	None

TABLE I: Species of regional Marine Mammals

marine mammal distribution and status in the Grand Passage area (adapted from Malinka, 2011 and Malinka *et al.*, 2015a). The "occurrence" refers to the number of sightings during whale tours, which cover a large area, on the order of 500 km^2, to the North and West of Grand Passage.

ii. Human activity

Traffic from small local vessels occurs throughout the year, but is particularly high during summer months due to increased recreational activity, including several whale watch vessels and various private small recreational craft. A number of local fisheries are based in Westport, which results in increased traffic during fishing seasons. A local diesel-electric car ferry crosses the channel approximately twice per hour in the daytime (and as needed during nighttime); the ferry idles dockside between crossings, typically around 35 minutes per hour at the Freeport wharf (Long Is.) and around 5 minutes per hour at the Westport wharf (Brier Is.).

B. INSTRUMENTATION

Given the diverse ecosystem in the Bay of Fundy, passive acoustic techniques had previously been investigated as a potential monitoring tool for marine mammals such as the North Atlantic right whale (Vanderlaan *et al.*, 2003); however, the shallow, narrow, high-flow environment in Grand Passage introduces additional constraints in the use of passive acoustic monitoring (PAM). An initial investigation of hydrophone methodologies, specifically targeting pseudonoise reduction, was conducted in 2012 (Malinka *et al.*, 2015b). Results indicated that flowshields of open cell foam on bottom-mounted hydrophones did not result in an unambiguous reduction in pseudonoise levels. Alternatively, drifter-based hydrophone methodology was found to be appropriate for ambient noise characterization. In the past several years, drifting hydrophones have been successfully used in several high energy sites, in the context of noise emissions from TEC devices (Bassett *et al.*, 2013; Robinson and Lepper, 2013). To expand upon the 2012 findings and the successful results at other sites, this methodology was modified to incorporate a drifting hydrophone array that would enable coherent processing and thus support 1) the identification of incoherent pseudonoise effects, 2) improved source characterization, and 3) investigation of second-order noise properties such as vertical coherence.

i. Moored hydrophones

Passive acoustic datasets were collected via bottom frame moorings over four deployment periods of weeks to months, at the locations indicated in figure 1. The instrumentation details and timeframe are provided in table II. The HF2014/2015 location provides long time series data for noise levels within the passage; the frame was moored in a sheltered location, such that pseudonoise effects could be minimized. The other moored hydrophone locations were outside the highest flow area, but were still subject to potential pseudonoise.

Map reference	Instrument	Deployment dates	F_s (ksps)	Data type	Storage
HF2012	icListen HF & LF	Sept. 6-25, 2012	512 (HF), 4 (LF)	FFT & WAV*	On-board
HF2014	icListen HF	Aug. 14-28, 2014	512	FFT & WAV	Cabled to shore
HF2015	icListen HF	Aug. 27-Nov. 22, 2015	512	FFT	On-board
ORCA2015	TR-ORCA	September 15-29, 2015	192	WAV	On-board

*TABLE II: Moored hydrophone deployment details. *Note: WAV files from the 2012 deployment were collected on a 1 minute per hour duty cycle (icListen HF).*

The icListen HF (Ocean Sonics) is equipped with an onboard digital signal processor that analyses data in real-time, reducing file size and enabling on-board storage of long time series data in "FFT file"

format. The files contain processed power spectral levels calculated using specified parameters (1024 points, Hanning window, 50% overlap, 250 segment ensemble average); details on the calculation of FFTs in digital acoustic time series are provided in section 2.C. With the hydrophone set at the maximum sampling rate, this results in power spectral estimates for each 0.25 seconds of data (0.5 seconds for 2014 deployment), with a frequency resolution of 500 Hz. Prior to computing the energy spectrum, a high-pass filter at approximately 2% of the analog bandwidth is applied to the data to remove the DC offset (A. Guimnan, Ocean Sonics, personal communication). This yields a lower frequency limit of 5 kHz at the maximum sampling rate of the instrument (512 kHz).

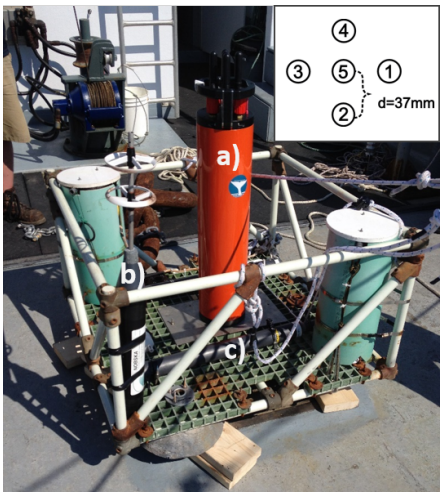

FIG. 2: ORCA2015 Frame and instrumentation: a) ORCA array and pressure case, b) Nobska MAVS; c) acoustic release; pressure sensor (RBR-Duo) behind MAVS, not visible in photo. Inset: configuration of 5 channels.

The 5-channel TR-ORCA hydrophone array (Turbulent Research) has a horizontal configuration with uniform inter-element spacing of 37 mm from center (channel 5) to outside (channels 1-4), as shown in figure 2; the configuration results in two orthogonal acoustic axes of length 74 mm across channels 1-3 and 2-4. The instrument housing contains sufficient battery power and storage capacity for continuous-sampling, autonomous deployments. The instrument was deployed for a two week period in September 2015, in a bottom-mounted configuration with additional instrumentation to measure flow speeds and hydrostatic pressure (figure 2).

ii. Drifting hydrophones

To minimize flow-induced pseudonoise contamination, and to improve the spatial resolution of soundscape characterization, drifter transects were conducted using a vertical array of two synchronized icListen HF hydrophones. The hydrophones were suspended at depths of approximately 3 and 4.5 m respectively (1.5 m array spacing). The drifter included bungee cables to reduce the vertical motion of the instruments and cylindrical wire brushes (additional drag) to account for the difference in surface flow versus water column flow, thus allowing the drifter to move mainly with the subsurface current.

Transects were completed over 5 days in September 2015, covering several flood and ebb tide periods during both spring and neap conditions; a total of 39 transects were conducted within Grand Passage, with drifter trajectories similar to the sample track provided in figure 1. The drifter was deployed and recovered via a rigid hull inflatable boat (RHIB), which drifted with engines off to minimize the vessel noise input during data collection.

iii. Supplementary data

Temperature and salinity profiles (for sound speed) and seabed video were collected from the RHIB during drifter deployments. Additional supplementary measurements and records used in data analysis include ADCP flow speed and backscatter (figure 1); diver video; Nobska MAVS flow speed measurements; pressure; meteorological records (hourly wind and 24 hour precipitation); and marine mammal observations.

C. ANALYSIS

Analysis of the hydrophone records was conducted in several stages, progressing from visual inspection to quantitative evaluation. The initial stage typically included calculation of power spectral density (PSD) from WAV data; generation of broadband, 1-6 hour spectrograms; and visual identification of relevant features (marine mammal vocalizations, vessel noise, sediment noise). Detailed assessment of specific observations was then based on established theoretical and empirical relations as well as concurrent datasets when available.

i. Spectral analysis

The WAV data were analyzed using spectral analysis techniques to evaluate the soundscape characteristics based on the distribution of acoustic energy in time and frequency. Power spectral densities were calculated using the ensemble-average of multiple overlapping, Hanning-windowed segments (Oppenheim *et al.*, 1999).

The array data were further analyzed to obtain second-order characteristics including phase, cross-spectral density (CSD), and coherence. The CSD between two signals is composed of a real part, the cospectrum, and imaginary part, the quadspectrum, corresponding to the in-phase component and out-of-phase component:

$$S_{xy}(f) = L_{xy}(f) - iQ_{xy}(f) \tag{1}$$

The phase, ϕ, is equal to:

$$\phi(f) = \tan^{-1}\left(\frac{\langle -Q_{xy}\rangle}{\langle L_{xy}\rangle}\right) = \phi_y - \phi_x \tag{2}$$

The coherence, Γ^2, is defined as:

$$\Gamma^2 = \frac{\langle S_{xy}\rangle^2}{\langle S_{xx}\rangle\langle S_{yy}\rangle} \tag{3}$$

The spectral and cross-spectral densities in the relations above are ensemble averages.

D. PSEUDONOISE

Pseudonoise is generated by non-acoustic turbulent pressure fluctuations passing over the hydrophone element, and is typically present at lower frequencies, with a theoretical maximum frequency dependent on mean flow speed U and the wavelength of the smallest turbulent spatial scales (Kolmogorov microscales) η_0^{-1} (Strasberg, 1979):

$$f = |U|\eta_0^{-1} \tag{4}$$

With microscales on the order of 0.3 mm (J. McMillan, personal communication) and peak mean currents of approximately 2.5 m/s in Grand Passage, theoretical pseudonoise would extend to 8 kHz. However, the effect of microscale pressures is expected to be reduced by averaging over the surface of the transducer, resulting in an upper limit of observed pseudonoise at $f_{max} < 0.5|U|D^{-1}$ (where D is the largest dimension of the receiver), above which intensities would decrease. The instruments used in the present study have a spherical piezoceramic element of diameter 1.27 cm (J. Abel, personal communication), resulting in a maximum value of 63 Hz.

Turbulence-induced pseudonoise will be at least partially incoherent across a hydrophone array, enabling the identification of pseudonoise via the inter-element coherence Γ^2 (equation 3). The flow speed dependence can be characterized from co-located flow measurements; this correlation has been conducted using the MAVS flow meter and ORCA acoustic measurements obtained at the ORCA2015 location. Coherence was calculated as the geometric mean of Γ^2 over acoustic axes 2-4 and 1-3, using both 1-minute and 10-second ensemble averages with a frequency resolutions of 1 Hz (192,000-point FFT), and a record length of 1,536,000 samples in each estimate. The coherence was evaluated for $1 < f < 500$.

E. NOISE GENERATION FROM MOBILE SEDIMENTS

Mobile sediment grains generate sound through rigid body radiation from interparticle collisions, and the cumulative effect of a broad grain size distribution and varying collision rates and speeds results in a

broadband SGN signature. The expected frequency range of the SGN contribution is based on an empirical relation developed by Thorne (1986) for the characteristic peak frequency of the broadband sound spectrum generated from collisions of equally-sized particles:

$$f \approx 0.182 \left[\frac{E}{\rho_s \left(1 - \sigma^2\right)} \right]^{0.4} \left(\frac{g^{0.1}}{D^{0.9}} \right) \tag{5}$$

where E is Young's modulus of elasticity, ρ_s is the density of the sediment grains, σ is Poisson's ratio, g is gravity and D is the grain diameter. The SGN sound pressure level increases with grain size, so the total SGN spectrum is a function of the grain size distribution within the mobile and immobile sediment fraction.

If a mobile particle collides with a stationary particle, sound will be produced. The mobility of unconsolidated seabed sediments is governed by the bottom stresses generated from boundary layer currents and can be represented by the friction velocity u_*, which is related to the current speed at height z above the bed by the Law of the wall,

$$U(z) = \frac{u_*}{\kappa} \ln \frac{z}{z_0} \tag{6}$$

where z_0 is the roughness length and $\kappa = 0.4$ is von Karman's constant.

The critical friction velocity u_{*c}, or threshold of sediment motion, can be estimated using the Shields parameter (equation 7) developed by Shields (1936) and a modified estimate (equation 8) presented by Hammond *et al.* (1984).

$$\theta_c = \frac{\tau_0}{(\rho_s - \rho) g D} \tag{7}$$

$$u_{*c} = 0.18 D^{0.2} \tag{8}$$

where $\tau_0 (= \rho u_*^2)$ is the critical bed shear stress, and ρ is the density of water, u_{*c} is in m/s and D is in m.

Drag coefficients from a location near the moored ADCP were reported to be 0.0061 and 0.0163 for the flood and ebb tides, respectively (McMillan *et al.*, 2013). In the present research, $U_{1\mathrm{m}}$ was calculated from the law of the wall, using a linear fit based on velocities at 2.11m and 4.11m height above bottom for the period of August 20-29; u_* was then calculated from $u_*^2 = C_{d1\mathrm{m}} U_{1\mathrm{m}}^2$. Histograms of friction velocity with predicted threshold values are presented in figure 3. These values indicate that sediment movement is likely for a range of sediment sizes for most of the tidal cycle.

The predicted threshold friction velocities, sediment percent mobility, and associated noise frequencies are presented in table III. Values were computed using the lowest grain size within a sediment class (i.e. $D_{finesand} = 0.125$mm, etc); percent mobility was based on the assumption that motion of sediments of a particular size would be initiated and maintained for any $u_* > u_{*c}$. The values of u_{*c} are higher using the Shields method, particularly at larger grain sizes. This is expected, as per the results of the Hammond et al. study.

The ebb/flood asymmetry in predicted mobility suggests a sediment noise regime with distinct flood and ebb tide characteristics.

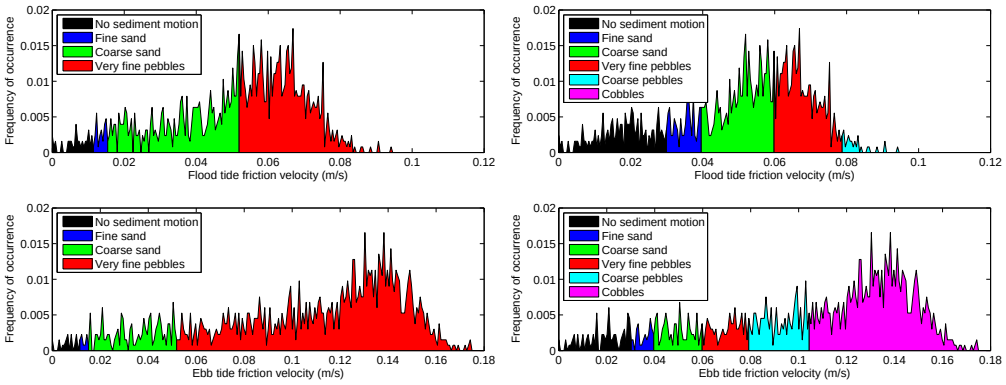

(a) Shields paramter estimate *(b) Hammond et al. estimate*

FIG. 3: Estimated friction velocity range and sediment mobility using two methods. The Shields parameter method estimates significantly higher u_{*c} and thus higher mobility for larger sediments.

Sediment Type	**u_{*c} (m/s)**		**Mobility: Flood (%)**		**Mobility: Ebb (%)**		**Frequency Range (kHz)**
	Shields	Hammond	Shields	Hammond	Shields	Hammond	
Fine Sand	0.011	0.03	97	84	99	93	150-1000
Coarse Sand	0.015	0.04	94	75	98	91	40-300
Fine Pebbles	0.052	0.06	56	38	85	83	6-40
Coarse Pebbles	0.11	0.08	0	2	0	74	2-10
Cobbles	0.22	0.1	0	0	0	59	0.5-3

TABLE III: Predicted sediment motion (portion of tidal cycle for which sediment is mobilized by the flow) and noise levels at the ADCP2014 location

F. RAINFALL NOISE

Rainfall events produce underwater sound through the formation of bubbles at the sea surface following impact from raindrops. Sound waves are generated by the collision of a raindrop with the water surface, through impact and rigid body vibrations, and by the free oscillations of entrained bubbles formed following drop impact (Franz, 1959). The impact noise is a broadband, short duration impulse (Medwin and Beaky, 1989), while the longer-duration noise produced by the bubbles formed following impact has a resonance frequency inversely proportional to the bubble diameter (Minnaert, 1933):

$$f_r = \frac{1}{2\pi a}\sqrt{\frac{3\gamma P}{\rho}} \tag{9}$$

where a is the bubble radius, γ is the ratio of specific heats of the bubble gas (=1.4 for air), P is the local pressure, and ρ is the density of air.

As demonstrated experimentally by Pumphrey et al. (1989), bubble entrainment, and thus bubble sound, does not occur with every drop impact but rather is related to a combination of drop size and impact velocity. The initial impact sound, by contrast, is generated with every drop, with an intensity that increases with velocity and drop size. The combination of factors contributing to a rain noise signature was investigated by Ma et al. (2005), who characterized acoustic observations and mechanisms based on rainfall parameters. It was also noted that tiny raindrops (<0.8 mm) do not have an observable acoustic signature.

Further to the characteristics presented in table IV, it has been found that rainfall noise is significantly

Drop size	Diameter (mm)	Acoustic mechanism	Frequency (kHz)
Small	0.8-1.2	No impact sound, many small bubbles	13-25
Medium	1.2-2.0	Weak impact sound, no bubbles	1-30
Large	2.0-3.5	Impact sound, large bubbles	1-35
Very large	>3.5	Loud impact sound, large bubbles	1-50

TABLE IV: Raindrop parameters and acoustic signature. Adapted from Ma et al.*, 2005*

influenced by wind speed, particularly for small raindrops; with a drop impact at oblique incidence, bubble formation becomes less likely and thus the resonance signal is diminished (Medwin *et al.*, 1990).

In addition to resonance effects, rain-induced bubbles can affect propagation characteristics under some conditions. Following an acoustically active period, quiescent entrained bubbles can act as scatterers; this is generally more relevant in the breaking-wave case, where wave-induced turbulence entrains bubbles and thus extends bubble-scatterer lifetime in the water column (Deane *et al.*, 2013). However, in heavy rainfall, subsurface bubble layer effects have been found to result in decreased sound levels at high frequencies through reduced sound speed and increased attenuation (Ma *et al.*, 2005).

G. MARINE MAMMAL VOCALIZATION BEARING

Acoustic measurements from the 5-channel horizontal hydrophone array (TR-ORCA) have been used in the identification of both odontocete and mysticete vocalizations. Low frequency ($<$ 1 kHz) sounds attributed to humpback whales are prevalent throughout the dataset; these relatively narrowband sounds (3 dB bandwidth typically $<$ 200 Hz, see Stimpert *et al.*, 2013), with a duration on the order of seconds, are well suited to bearing determination via beamforming. The bearings of 129 mammal sounds were determined using S_{xy} (equation 1), computed for channels 4-2 and 1-3, representing approximately N-S and E-W directions, with 19200-point segments and a record length of 8 segments (0.8 seconds) in each estimate, providing 15 equivalent degrees of freedom. The bearing was then obtained using the two methods described below.

i. Beamforming

The time-synchronized array enables the application of beamforming algorithms, which steer the array beam pattern in azimuth. In this method, the cross-spectral density matrix is weighted by a vector w whose phase is equal to the phase difference between two spatially separated receivers at a given source angle θ. The beamformer output is maximized when the CSD is in-phase with w; i.e., at the value of θ corresponding to the true source angle θ_T. The bearing from each transducer pair has a 180 degree ambiguity. The sign of the phase difference from the orthogonal pair can be used to resolve the ambiguity and obtain results for $0 < \theta < 360°$. The main advantage of beamforming lies in the amplification of signal intensity, improving the ability to resolve source angle where the signal to noise (SNR) ratio is low.

ii. Phase difference

In the second method, the source angle θ is calculated directly from the spatial phase difference, $\Delta\phi$, of a plane wave of the form $\exp(\vec{k} \cdot \vec{x} - \omega t)$ arriving at two receivers in a hydrophone pair. Removing the time dependence, this becomes $\phi = \vec{k} \cdot \vec{x}$, which is related to the inter-element spacing d and source angle θ. The advantage of this method is improved computational efficiency, as θ can be calculated directly without the application of a "beam-steering" loop. However, the method is limited to cases where the SNR is sufficiently high. Phase difference analysis has been implemented here only for those low-frequency mammal sounds with relatively high SNR.

3. RESULTS

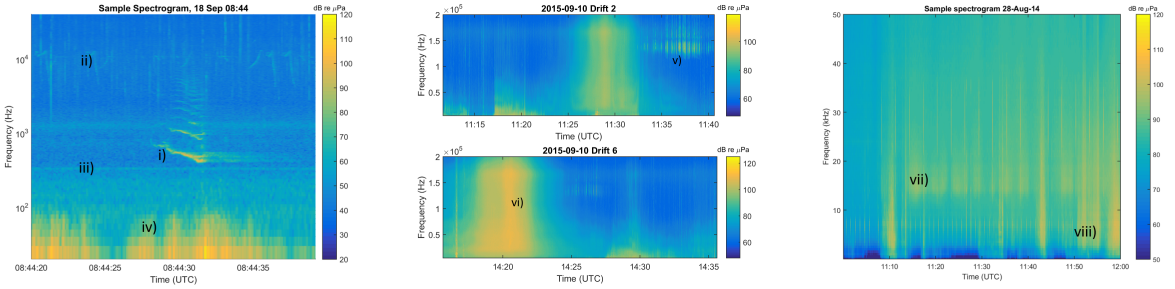

(a) ORCA hydrophone *(b) Drifting hydrophone* *(c) HF2014 moored hydrophone*

FIG. 4: Sample spectrograms from deployments as indicated. Identified signals: i) humpback whale; ii) Atlantic white-sided dolphin; iii) Vessel (rotating machinery); iv) Pseudonoise; v) Harbour porpoise; vi) SGN; vii) & viii) Rain. Spectrogram in b) was computed from FFT data; a) and c) were computed from WAV data with window lengths of a:19200 and c:2048 points.

Visual inspection has provided a qualitative assessment of the soundscape both within Grand Passage and in the coastal region North of the passage. Figure 4 provides a sample of visually-identified signals, based on known source and sound characteristics. Results are presented in the following sections.

A. PSEUDONOISE

Because pseudonoise is incoherent, and has highest intensity at low frequencies, the average value Γ^2 in the band $0< f < 500$ Hz is used as a proxy for the presence or dominance of pseudonoise. The highest coherence is observed during low flow periods, as shown in figure 5, with values decreasing significantly with increasing flow speed. As shown in figure 5, the variation in coherence is strongly aligned with local flow changes, on long time scales (on the order of hours). This has implications for monitoring of low-frequency marine mammal sounds, such as those produced by fin or minke whales, as pseudonoise masking becomes increasingly probable at higher flow speeds.

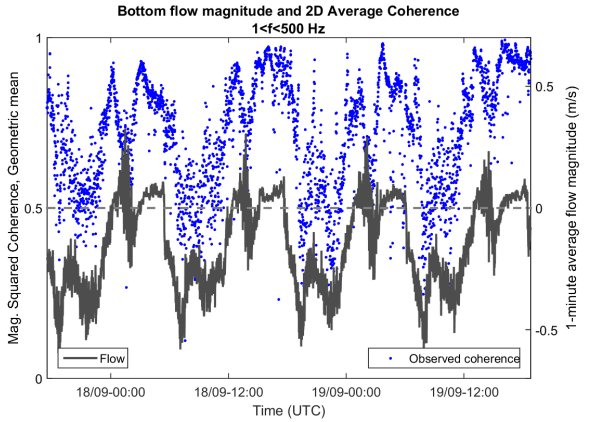

FIG. 5: 1-minute average coherence (average over the band 10-500 Hz) and flow speeds. The coherence has a cyclic signature with tidal periodicity and irregular amplitude variation that is strongly correlated with flow speed.

An examination of pseudonoise and flow speed on shorter time scales (10 second averages) found that the correlation did not hold at this scale; this could be due to orientation effects, where flow measurements in the wake of the hydrophone may be inaccurate on short time scales.

B. ANTHROPOPHONY

Moored hydrophones frequently registered broadband, intense noise from passing vessels. Visual inspection of these datasets was used to minimize the contamination of results based on band- or time-averaging. The local ferry is a dominant source of vessel noise, with detectable band-average sound up to the 128 kHz (see figure 10). High noise levels are generated at irregular intervals by whale-watching boats (outboard and inboard motors) that travel through the passage daily during the summer season, as well as by 10-20m fishing vessels and small recreational craft.

Long distance shipping noise, which is typically observed at low frequencies (Wenz, 1962), is not detectable in Grand Passage, despite large vessel traffic in the outer Bay of Fundy. At the Northern channel entrance, both local, broadband and long-range, narrowband vessel noise (as shown in figure 4a) has been measured at the ORCA mooring. The propagation of distant vessel noise into Grand Passage is restricted by the shallow bathymetry in the channel region. In addition, low frequency noise from sources within the Passage would likely mask long range shipping noise (i.e. vessel noise at frequencies of order 100 Hz).

C. BIOPHONY

Within Grand Passage, harbor porpoise sounds are significantly more common than any other detected mammal sound. Outside the passage, where noise contamination from vessel traffic is lower, cetacean sounds at sub-kHz frequencies have been detected: in the September 2012 record, this included right whales and humpback whales, and in the 2015 record, humpback and minke whales. No right whale sounds were detected in 2015, whereas the detection rate for the 2012 period was ~ 0.1 per minute for the 1 minute per hour duty cycle WAV data collection. The small numbers of right whales in the Bay of Fundy in 2015 is the subject of ongoing research at several institutions.

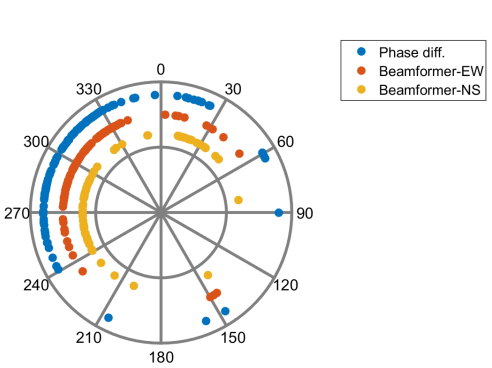

(a) Low frequency mammal sounds source bearing from ORCA2015 location, 17-19 September.

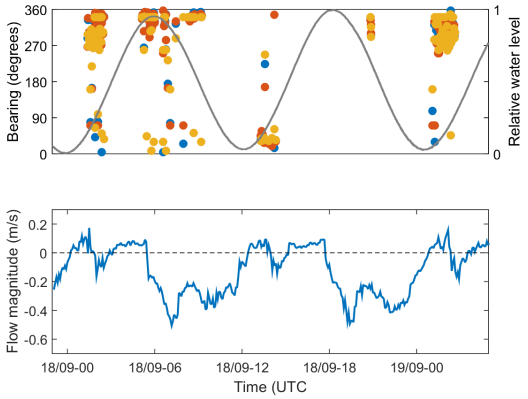

(b) Time series of detections and bearing with water level and flow variation.

FIG. 6: Distribution of bearing calculated for 129 humpback whale vocalizations. The distribution agrees well with past vessel-based observations of marine mammals in the region (Malinka et al.*, 2015a).*

For each of the 129 identified humpback vocalizations, source bearing was computed using the two methods described in section 2.C. Beamformer-NS values were generated from the approximately North-South acoustic axis between channels 4 and 2, and Beamformer-EW values were generated from the East-West axis between channels 1 and 3. Phase difference values are the mean value of θ calculated from ϕ_{42} and ϕ_{13}. The computed bearings were corrected for the ORCA's heading and the local magnetic declination of 16.87 degrees.

The distribution of source bearings is broad (figure 6), but concentrated mainly in the northwest quadrant: i.e. toward Grand Manan basin and the entrance to the Bay of Fundy, which is where the whales are most frequently visually observed. Results from the two methods show good agreement, indicating that for the humpback sounds dataset, the computationally efficient phase difference technique is an effective method for bearing analysis.

The detected whale vocalizations are temporally distributed in groups separated by periods of several hours. To examine this distribution in relation to the tidal cycle, the detections are plotted together with pressure and flow in figure 6b. While the record length is short, it is observed that there are two significant

groups of detections (approximately 30-40 vocalizations in each group) during both overnight flood tides (near 00:00-03:00 local time). This could be an indication of improved visual signal identification due to reduced masking by broadband local vessel traffic noise.

Harbor porpoise sounds have been identified in the HF2014/2015 moored hydrophone records and 2015 drifting hydrophone records. The drifting vertical array enables examination of second-order characteristics, and it has been found that porpoise noise identification is significantly improved using coherent processing. Spectra from drifter recorders were calculated with a frequency resolution of 10 Hz, 50% overlap, and ensemble averages of 4 segments per estimate. The coherence was then calculated from equation 3. A comparison of harbor porpoise vocalizations identified through both intensity and inter-element coherence is provided in figure 7. The increase in visual identification using a coherent processing approach is immediately apparent, due to the low coherence of background noise; this noise is predominantly SGN in this frequency range, which, as a superposition of sound radiated from multiple collisions with a wide variance of source signatures and amplitudes, is relatively non-stationary compared to a sustained deterministic source (harbor porpoise click train). Thus, over the appropriate time window, the porpoise vocalizations are enhanced, while the SGN noise is suppressed in the coherency spectrum.

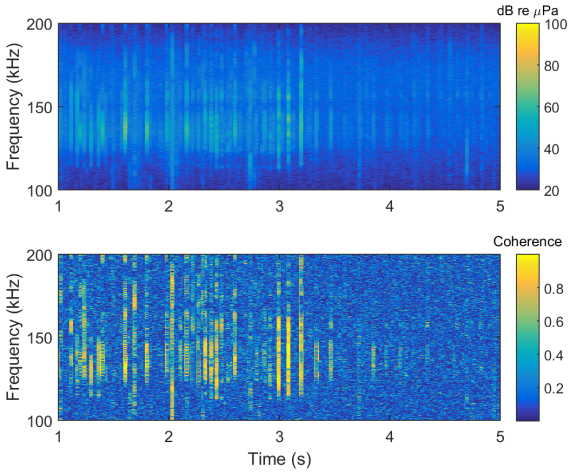

FIG. 7: Identification of harbor porpoise sounds through intensity and coherence. The porpoise signals have significantly higher coherence than the background noise (primarily SGN), and thus the signal-to-noise ratio is improved in the coherence spectrum.

This finding has implications for detection of marine mammal signals in the passage, particularly at high frequencies where intense SGN can decrease the signal to noise ratio or where propagation is constrained by higher losses as compared to low-frequency mammal signals.

D. GEOPHONY

i. Sediment-Generated Noise

In the northern end of the passage, and diminishing southward as the channel widens, SGN is a dominant source over a wide bandwidth. The drifting hydrophone results (figure 4b) show a peak SGN intensity in a region of known "gravel waves", where diver video shows the sediment to be a loosely compacted mix of gravel/sand/shell hash. Seismic profiles found the gravel/sand layer to be 5-10 m thick in this region, transitioning to glacial till as the channel widens (figure 8). The location of maximum SGN is consistent over all drifting records, for both flood and ebb tides and in spring and neap conditions.

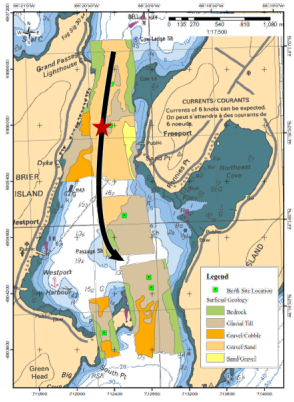

FIG. 8: Representative ebb tide drifter track and location of peak SGN intensity (map adapted from CSR, 2014).

As shown in figure 9, the SGN spectra from the drifting hydrophones differ significantly from the commonly observed open-ocean ambient noise slope of $f^{-5/3}$ at high frequencies (Wenz, 1962); recorded noise levels are elevated in the 10-100 kHz band, due to the increased generation of acoustic energy by sediment collisions. The figure also shows a consistent difference in intensity recorded by the drifting phones compared to the moored phone, likely due to transmission loss; the location of maximum SGN is approximately 400 m west of the mooring location.

The flood/ebb flow asymmetry results in an asymmetric SGN signature. The recorded intensities are higher during the ebb tide, particularly for frequencies of $f < 10$ kHz; this agrees with predictions presented

in figure 3, which suggested a higher fraction of the larger-grained sediments should be mobilized during the ebb. Figure 10 shows the band-average SGN over a tidal cycle (neap conditions); flow speeds are depth-averaged, and both flow and noise are 5-minute averages.

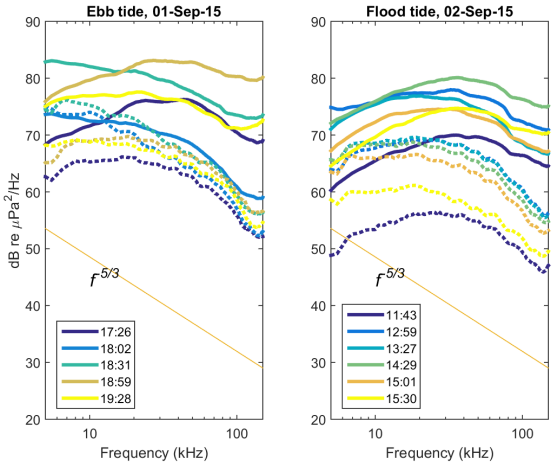

FIG. 9: Comparison of SGN spectra from ebb and flood tides on two consecutive days, from the peak SGN intensity recorded during each drift; spectra are two-minute ensemble averages from the lower drifting phone (solid lines) and corresponding records at the same time taken at the moored hydrophone (dashed lines). The spectra show a significant deviation from the $f^{-5/3}$ relation. Ebb tide spectra from the drifting phone show increased acoustic energy and peak at lower frequencies compared to flood tide.

There is a strong correlation between noise levels and flow speed, which is particularly pronounced during the peak ebb currents near the 03:00 mark. During ebb conditions, noise levels are at a maximum over a wide bandwidth (8-32 kHz), whereas flood conditions show a peak in the 32 kHz band. As shown in table III, the higher friction velocity during the ebb tide is predicted to mobilize pebble-size grains for a longer time interval compared to flood (38 and 83 per cent of flood and ebb tides, respectively, based on the Hammond estimate), which would result in increased noise over the 6-40 kHz bandwidth. At higher frequencies, the flood/ebb noise levels are nearly equal, which again agrees with predictions, since high rates of sand grain mobilization are expected during both ebb and flood.

Figure 10 also highlights the significance of the SGN contribution. The intensity difference between low flow periods (slack tide) and peak flow is on the order of 20 dB; this is the measured difference at the moored hydrophone location, which is known to be sheltered from the strongest flows.

ii. Rain

A rainfall event with light winds occurred during the HF2014 deployment, enabling an assessment of rain noise in the absence of wind waves. The total 24 hour rainfall was 4.6 mm, but a rain signature is identifiable (figure 4c), based on known characteristics. The WAV data was high-passed filtered at 1000 Hz, to reduce vessel noise contamination, and was processed with a frequency resolution of 250 Hz. Sample 10-second spectrograms were visually examined to ensure the sample was not contaminated by local vessel noise, and a 10-second average PSD was calculated for comparison to rainfall noise spectra.

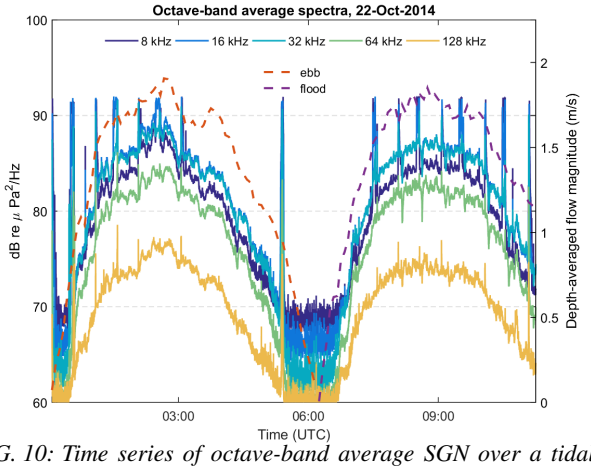

FIG. 10: Time series of octave-band average SGN over a tidal cycle during neap conditions. Ebb tide shows consistently higher levels, particularly in the 8-32 kHz bands. The observed flow speed peak at 03:00 correlates well with recorded noise levels in all bands. The sporadic noise peaks are caused by the local ferry, running as needed during night hours.

The resulting spectra for the rain event are shown in figure 11, indicated by the solid lines. Two rain cases are shown: case 1, recorded at 11:15, and case 2, recorded at 11:52. Also shown are the spectra on the previous day (dashed lines) recorded during the same tidal flow stage (i.e., time-shifted by -50 minutes), which exhibit the characteristic SGN signature. Both rain noise cases deviate significantly from the SGN spectra at frequencies below 30 kHz. The first case (rain 1) shows both a defined peak and a broadband intensity increase over 5-100 kHz; at its peak,

the small raindrop noise results in a PSD increase of approximately 15 dB, falling to $\sim$ 3 dB at $f > 50$ kHz. This indicates the resonance effect of a given bubble size range created by small raindrops ("type II" bubbles after Ma *et al.*, 2005), which introduce sound at 13-25 kHz, as well as the less significant impact noise generated over a wide frequency band. The previous-day spectra were recorded during flows of $\sim$ 1 m/s (depth-averaged), indicating that SGN intensity would be below its peak value. Comparing case 1 rain spectra to the higher intensity SGN recorded during case 2 rain, it is evident that this noise would not be distinguishable above SGN for $f > 20$ kHz.

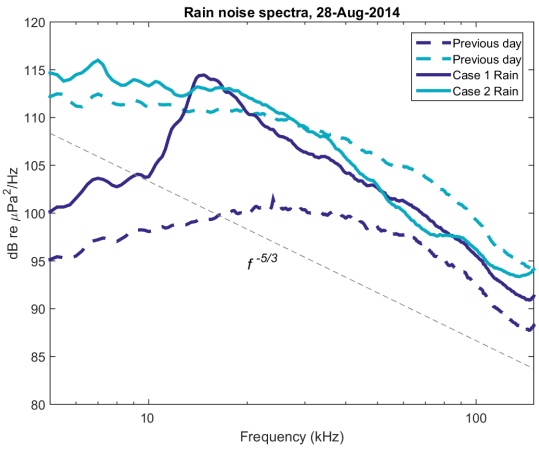

FIG. 11: 10-second average spectra recorded at HF2014 during a rainfall event with low winds. The cases have been characterized as 1) small raindrop noise, identified by a peak at 14-20 kHz due to small bubble resonance; and 2) heavy rain/large raindrop noise, identified through a broadband increase in intensity and a steep negative slope at $f > 30$ kHz.

Case 2 rain, which occurred during peak flow speeds ($\sim$ 2 m/s), shows a small increase in intensity of approximately 2 dB over the 5-20 kHz band. Above 20 kHz, however, the spectral slope begins a steep decrease ($\sim f^{-3}$), greater than the typical SGN slope as well as the Knudsen wind-driven slope. The lack of a distinctive peak in this case suggests that raindrops were of a medium-large size, resulting in a wider range of potential bubble sizes that generate sound over a wider bandwidth; in addition, impact noise is louder for larger drops (see table IV), which could further increase sound levels over this frequency range. The steep slope, and decrease in PSD compared to the previous day, indicates attenuation of SGN at high frequencies. We suggest that this attenuation could be due to the characteristic subsurface bubble layer associated with heavy rainfall (Ma *et al.*, 2005).

4. CONCLUSIONS

The soundscape in Grand Passage, Nova Scotia has been assessed based on anthropo-, bio-, and geophonic contributions. To mitigate the challenges associated with passive acoustic data collection in high flow tidal environments, and to contribute to the development of a comprehensive approach to soundscape characterization that addresses the spatial and temporal variability of the ambient noise field, the research approach implemented several complementary measurement and analysis techniques. In addition, the research assimilated results from previous studies as well as concurrent datasets to conduct an assessment that is optimized for this particular environment. The soundscape is significantly influenced by the high-energy flows and diverse biological and human activity. These flows introduce low-frequency non-acoustic pseudonoise contamination that can mask acoustic signals; an evaluation of pseudonoise effects has found a strong correlation with flow speeds on time scales of hours. Biological sounds have been identified over a wide frequency range from mysticete and odontocete populations; the detection of these sounds is likely influenced by vessel noise masking and by incoherent high-frequency background noise predominantly due to mobile seabed sediments. The strong currents mobilize seabed sediments in the passage, resulting in a broadband, intense signal with tidal variability spatially correlated to seabed sediment properties. The high levels of SGN introduce constraints for detection and monitoring of other local sounds including marine mammal vocalizations or a tidal turbine acoustic signature, but the predictable nature of the observed temporal and spatial variability provides a foundation for statistical evaluation of potential detection rates. Finally, the results show that rainfall events can influence the broadband soundscape through both generation and propagation effects, introducing additional variability that has implications for signal detection.

REFERENCES

Bassett, C., Thomson, J., and Polagye, B. (**2013**). "Sediment-generated noise and bed stress in a tidal channel", Journal of Geophysical Research: Oceans 2249–2265.

CSR (**2014**). "2014 seabed analysis - Grand Passage, Petit Passage, and Digby Gut", Technical Report, Fundy Tidal Inc.

Deane, G. B., Priesig, J. C., and Lavery, A. C. (**2013**). "The suspension of large bubbles near the sea surface by turbulence and their role in absorbing forward-scattered sound", IEEE J. Oceanic Eng. **38**, 632–641.

Erbe, C., Verma, A., McCauley, R., Gavrilov, A., and Parnum, I. (**2015**). "The marine soundscape of the Perth Canyon", Prog. Oceanog. **137**, 38–51.

Franz, G. (**1959**). "Splashes as sources of sound in liquids", J. Acoust. Soc. Am. **31**, 1080–1096.

Hammond, F., Heathershaw, A., and Langhorne, D. (**1984**). "A comparison between Shields' threshold criterion and the movement of loosely packed gravel in a tidal channel", Sedimentology **31**, 51–62.

Hay, A., Karsten, R., Trowse, G., Morin, D., Webster, T., McMillan, J., O'Flaherty-Sproul, M., Schillinger, D., Cheel, R., Marshall, E., Crowell, N., and Collins, K. (**2013**a). "Southwest Nova Scotia resource assessment: Final report", Technical Report, Offshore Energy Research Association.

Hay, A. E., McMillan, J., Cheel, R., and Schillinger, D. (**2013**b). "Turbulence and drag in a high Reynolds number tidal passage targetted for in-stream tidal power", Oceans 2013 San Diego 1–10.

Ma, B., Nystuen, J., and Lien, R. (**2005**). "Prediction of underwater sound levels from rain and wind", J. Acoust. Soc. Am. **117**, 3555–3565.

Malinka, C. (**2011**). "In-stream tidal energy devices and marine mammals in Southwest Nova Scotia: Review of possible impacts and proposed mitigative strategies", Technical Report, Fundy Tidal Inc.

Malinka, C., Brown, M. W., Trowse, G., Inney, B., and Zetterlind, V. (**2015**a). "Marine sightings report", Technical Report, Offshore Energy Research Association.

Malinka, C., Hay, A., and Cheel, R. (**2015**b). "Toward acoustic monitoring of marine mammals at a tidal turbine site: Grand Passage, NS, Canada", Proc. of EWTEC 2015 1–10.

McMillan, J., Schillinger, D., and Hay, A. (**2013**). "Southwest Nova Scotia resource assessment volume 3: Acoustic Doppler current profiler results", Technical Report, Offshore Energy Research Association.

Medwin, H. and Beaky, M. M. (**1989**). "Bubble sources of the Knudsen sea noise spectra", J. Acoust. Soc. Am. **86**, 235–248.

Medwin, H., Kurgan, A., and Nystuen, J. A. (**1990**). "Impact and bubble sound from raindrops and normal and oblique incidence", J. Acoust. Soc. Am. **88**, 413–418.

Minnaert, M. (**1933**). "On musical air-bubbles and the sounds of running water", Philosophical Magazine **16**, 235–248.

Oppenheim, A. V., Schafer, R. W., and Buck, J. R. (**1999**). *Discrete-Time Signal Processing* (Prentice-Hall, Upper Saddle River, NJ).

Robinson, S. and Lepper, P. (**2013**). "Scoping study: Review of current knowledge of underwater noise emissions from wave and tidal stream energy devices", Technical Report, The Crown Estate.

Shields, A. I. (**1936**). "Application of similarity principles and turbulence research to bed-load movement", Mitteilungen der Preussischen Versuchsanstalt fur Wasserbau und Schifbau, Ott, W.P. and van Uchelen, J.C. (translators), California Institute of Technology.

Stimpert, A. K., Au, W. W. L., Parks, S. E., Hurst, T., and Wiley, D. N. (**2013**). "Common humpback whale (*Megaptera Novaeangliae*) sound types for passive acoustic monitoring", J. Acoust. Soc. Am. **38**, 476–482.

Strasberg, M. (**1979**). "Nonacoustic noise interference in measurements of infrasonic ambient noise", J. Acoust. Soc. Am. 1487–1493.

Thorne, P. (**1986**). "Laboratory and marine measurements on the acoustic detection of sediment transport", J. Acoust. Soc. Am. **80**, 899–910.

Vanderlaan, A. S. M., Hay, A. E., and Taggart, C. T. (**2003**). "Characterization of North Atlantic right-whale (*Eubalaena Glacialis*) sounds in the Bay of Fundy", IEEE J. Oceanic Eng. **28**, 164–173.

Wenz, G. M. (**1962**). "Acoustic ambient noise in the ocean: Spectra and sources", J. Acoust. Soc. Am. **34**, 1936–1956.

Williams, R., Ashe, E., Blight, L., Jasny, M., and Nowlan, L. (**2014**). "Marine mammals and ocean noise: Future directions and information needs with respect to science, policy and law in Canada", Marine Pollution Bulletin **86**, 29–38.